Hydrogeophysical study of the heterogeneous unsaturated zone of a stormwater infiltration basin

David GOUTALAND
Thierry WINIARSKI *
Université de Lyon, LSE - ENTPE, Vaulx-en-Velin, France
Rafael ANGULO-JARAMILLO
Université de Lyon, LSE - ENTPE, Vaulx-en-Velin, France
LTHE, CNRS UMR 5564, Grenoble, France
Laurent LASSABATÈRE
LCPC, Bouguenais, France
Grégory BIÈVRE
LRPC, Autun, France
LGIT, CNRS UMR 5559, Grenoble, France
Jean-François BUONCRISTIANI
Université de Bourgogne, Biogéosciences, CNRS UMR 5561, Dijon, France
Jean-Sébastien DUBÉ
École de technologie supérieure de Montréal, Montréal, Canada
Ali MESBAH
Université de Lyon, LGM - ENTPE, Vaulx-en-Velin, France
Henri CAZALETS
Université de Lyon, LSE - ENTPE, Vaulx-en-Velin, France

*CORRESPONDING AUTHOR:
Thierry WINIARSKI
winiarski@entpe.fr

ABSTRACT

The reliance upon stormwater infiltration systems as alternative sewerage techniques is quite frequent in urban settings. The long-term environmental impact of urban stormwaters on groundwater and subsoils is not however known. An evaluation of this impact necessitates reliable knowledge of the subsurface structures and their hydraulic properties. By means of a hydrogeophysical approach based on characterization at the lithofacies scale, which overlaps with both a geophysical characterization (Ground Penetrating Radar, electrical resistivity) of the sedimentary structures and an *in situ* hydraulic characterization (Beerkan infiltration tests), a realistic hydrostratigraphic model of a glaciofluvial deposit underlying a stormwater infiltration basin was built. This model reflects sedimentary and hydraulic heterogeneities at the hydrofacies scale. The two-dimensional numerical modeling of unsaturated flows serves to illustrate the impact of sedimentary heterogeneities on water content distribution within the unsaturated zone. Matrix-free gravel hydrofacies can act like preferential flow paths or induce capillary barrier effects leading to lateral flow patterns.

Étude hydrogéophysique de la zone non saturée hétérogène d'un bassin d'infiltration d'eaux pluviales

RÉSUMÉ

Le recours à des systèmes d'infiltration d'eaux pluviales comme techniques d'assainissement alternatives est fréquent en milieu urbain. L'impact environnemental à long terme des eaux pluviales sur le milieu souterrain (nappe et sous-sols) n'est cependant pas connu. L'évaluation de cet impact requiert au préalable une connaissance fiable des structures de subsurface et de leurs propriétés hydrodynamiques. Par une approche hydrogéophysique fondée sur une caractérisation à l'échelle du lithofaciès, couplant d'une part une caractérisation géophysique (radar géologique, résistivité électrique) des structures sédimentaires et d'autre part une caractérisation hydrodynamique *in situ* (essais d'infiltration Beerkan), un modèle hydrostratigraphique réaliste d'un dépôt fluvioglaciaire sous-jacent à un bassin d'infiltration d'eaux pluviales a été construit. Ce modèle traduit l'hétérogénéité sédimentaire et hydrodynamique à l'échelle de l'hydrofaciès. La modélisation numérique bidimensionnelle des écoulements en conditions non saturées illustre l'impact des hétérogénéités sédimentaires sur la répartition des teneurs en eau dans la zone non saturée. Les hydrofaciès de graviers sans matrice peuvent agir comme des chemins préférentiels d'écoulement, ou induire des effets de barrière capillaire conduisant à des flux d'écoulement latéraux.

INTRODUCTION

Surface geological formations such as alluvial formations are often generated by processes of erosion, transport and sedimentation, causing considerable heterogeneity in hydraulic parameters

(hydraulic conductivity, porosity). Knowledge of the distribution and variability of these parameters is key to estimating flow fields. The spatial variability in flow directions and hydraulic conductivity is correlated with both the composition and dimension of sedimentary structures, which themselves are correlated with the dynamic of the former fluvial systems. Hydraulic conductivity is typically anisotropic in such formations; its vertical component is often smaller than its horizontal one within sedimentary aquifers **[1]**. Anderson showed the need to estimate hydraulic conductivity variations between representative hydrogeological facies and then develop statistical descriptions in order to represent these variations **[2]**. Such details may prove necessary in describing groundwater flows at the local scale. Subsurface investigations, such as pumping tests, yield parameters measured at a larger scale than the average size of sedimentary structures, making it difficult to obtain an image of the geometry and heterogeneities at the local scale **[3]**. Moreover, these investigations do not incorporate the lateral continuity of shallow structures. It is essential however to generate this type of information, particularly as regards three-dimensional structures. These heterogeneities taken as a whole represent a major obstacle when modeling flows in the unsaturated parts of aquifers **[4]**.

In France, a sizable proportion of urban zones is located on shallow formations. As an example, 72% of the population within the Rhône catchment basin resides on alluvial deposits (either glaciofluvial or fluvial), while these deposits represent just 25% of the total surface area. This urbanization has created the need for many hydraulic structures such as stormwater infiltration basins, drainage ditches and infiltration wells. At the scale of these facilities, sedimentary heterogeneities can cause non-homogeneous flows. Furthermore, stormwater may be loaded in contaminants of urban origin, thereby inducing a risk for both soils and groundwater resources.

The role of sedimentary data in flows often gets neglected when building transport models; yet such information, based on geological and geophysical knowledge of varying types, needs to be integrated **[5]**. A number of research projects over the past several years have sought to employ geophysical techniques, e.g. Ground Penetrating Radar (GPR), to describe the sedimentary architecture **[3,4,6-9]**. These projects have shown that sedimentary structures are responsible for flow heterogeneity. Winiarski *et al*. **[10,11]** demonstrated that the natural sedimentary heterogeneity of a glaciofluvial deposit underlying a stormwater infiltration basin exerts an impact on flows in the unsaturated zone. Klingbeil *et al*. **[12]** established a correlation between lithofacies and hydrofacies. The term hydrofacies is used herein for homogeneous, yet not necessarily isotropic, sedimentary units, which are significant from a hydrogeological standpoint **[2]**. Walter *et al.* defined various preferential flow mechanisms, includinsg those induced at the interface between two different soil layers **[13]**. Infiltration front instability at the interface between two layers of different textures can engender digitation phenomena within the lower layer **[14]**. Development of a capillary barrier at the interface between an upper layer composed of a relatively fine-grained soil and a lower layer with a coarser particle size distribution generates non-vertical flow along the interface, referred to as *funneled flow* **[15-17]**.

Using the example of the Eastern Lyon infiltration basin study, a hydrogeophysical method based on overlapping sedimentological, geophysical and hydrodynamic examinations will be proposed herein for the purpose of characterizing the hydrostratigraphic units capable of giving rise to preferential flow paths **[18]**. Results stemming from two geophysical techniques well adapted to the test scale, i.e. Ground Penetrating Radar and electrical resistivity, will be presented. A hydraulic characterization of the lithofacies encountered has also been conducted in the aim of proposing a geometric model for distributing subsoil hydraulic characteristics. Lastly, a suggested two-dimensional flow model within the unsaturated zone will be introduced to illustrate the impact of these heterogeneities and evaluate the existence of preferential flow paths.

Description of the study site

The study site is an infiltration basin, set up to the east of the Lyon metropolitan area, that captures stormwater stemming from a 185-ha catchment area encompassing an industrial park located south of the city of Chassieu **(see Fig. 1)**. This basin, 1 ha in surface area, has been excavated into glaciofluvial deposits whose average saturated hydraulic conductivity varies between 7.10^{-3} and 9.10^{-3} m.s^{-1} **[19]**. These deposits overlie a tertiary molassic *substratum* at a depth of approximately 35 m. The alluvial aquifer lies at a depth of 13 m below the infiltrating surface of the basin. The infiltration basin is preceded by a retention-decantation basin that serves to decant suspended matter. The infiltration basin is called the Django-Reinhardt (or DjR) basin. These two basins constitute observation sites for the Field Observatory for Urban Water Management (Observatoire de terrain en hydrologie urbaine, or OTHU), a research federation set up within the Lyon metropolitan area to collect in situ data in order to evaluate environmental risks tied to urban stormwater, in the aim of protecting and restoring soils and groundwater resources, as well as proposing to local decision-makers strategic guidelines for managing stormwater **[20]**.

Characterization methods

Sedimentary heterogeneities can exert, at the structural scale, an impact on unsaturated flows. It is proposed herein to evaluate this impact by using a numerical flow model. The modeling process

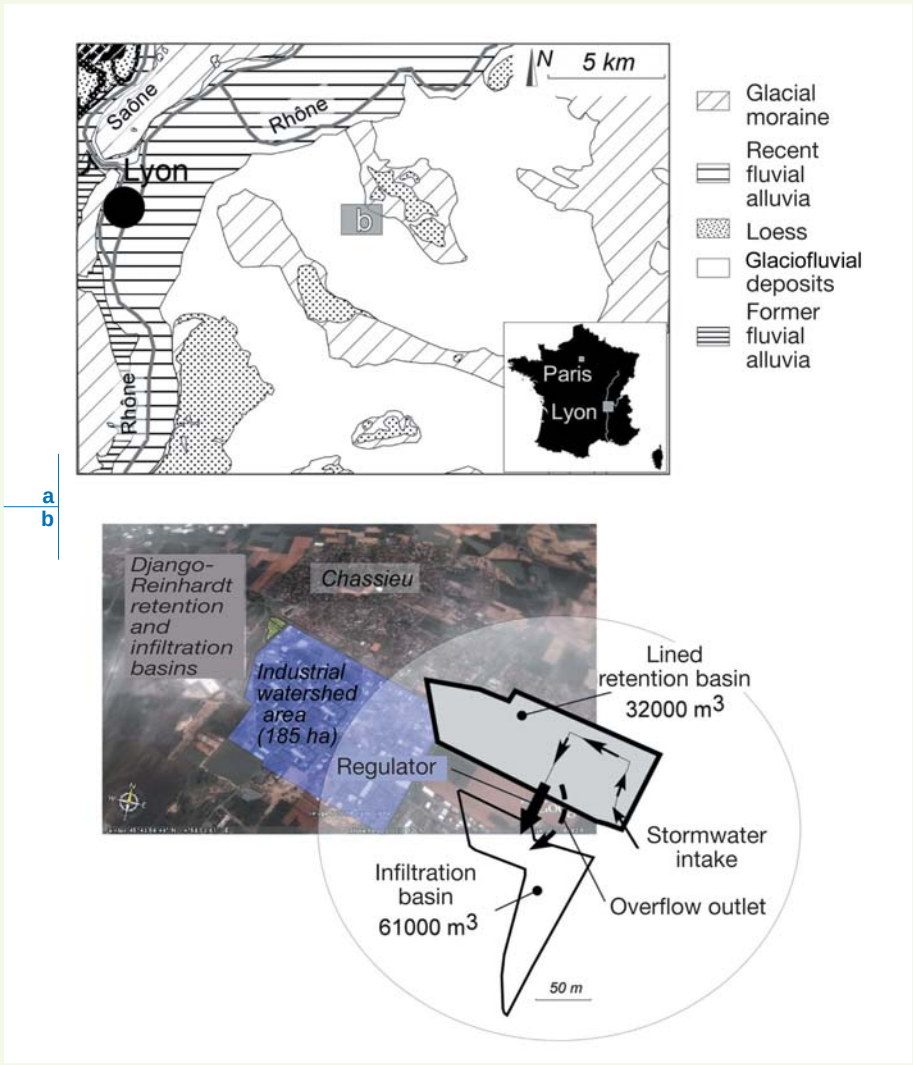

figure 1
- a: Geological context and position of the studied stormwater infiltration basin;
- b: Operating diagram for both the Django Reinhardt (DjR) retention/decantation basin and infiltration basin constituting the outfall of a 185-ha industrial watershed area

involves two scales of heterogeneities: the textural and structural scales. At the textural or mesoscopic scale **[18]**, homogeneous hydraulic properties may be assigned to hydrogeological units, whose characteristic dimensions lie in the centimeter to decimeter range. The structural or macroscopic scale **[18]** in turn corresponds with subsoil structure geometries at a scale dimension in the metric to decametric range, i.e. at the scale of the distribution of hydrogeological units between one another. The architecture of the depositional elements influences connectivity of these hydrological units between one another **[18]**. Both scales are distinguished in this paper.

› Textural scale: Lithofacies

Alluvial glaciofluvial deposits are characterized by a textural heterogeneity derived from the phases of erosion, transport and sedimentation that have led to the current configuration of lithological units. In the following discussion, the term lithofacies will be used in reference to lithological units of the glaciofluvial deposit, which corresponds to a genetic unit, i.e. formed by a homogeneous process of transport and sedimentation **[21]**.

In order to highlight the textural heterogeneity of the glaciofluvial deposit, two trenches were excavated using a power shovel in the infiltration basin. A sedimentological description and sampling were conducted on a vertical sidewall of these trenches, while the opposite sidewall was banked so as to facilitate photographic and sampling work. These trenches have been identified on **Figure 2**; the trench dug in the northwestern zone of the basin, called Zone A, was 13.5 m wide and 2.5 m deep, while the trench in the southeastern zone of the basin, i.e. Zone B, had a 3-m depth and 15-m width. Each sidewall was successively:

– described from a sedimentological perspective, with the lithofacies being inventoried; and
– sampled: the sidewall was divided into 1.5 m-wide sections within which sampling was performed at the level of each lithofacies, for the purpose of conducting a grain size analysis.

The choice of section width was made in a way that avoided an overrepresentation of any single lithofacies (meter-long lateral extension of the lithofacies). The textural heterogeneity was characterized using Miall's code of sedimentological classification **[22]**, adapted to glaciofluvial deposits by Heinz *et al*. **[21]**. This code, shown in **Table 1,** is composed of a sequence of letters (I_1 i_2 i_3, i_4) indicating the grain size distribution of the major elements (I_1: *G* for gravels, *S* for sands), component fabric (i_2: *c* for clast-supported, m for matrix-supported, - for lithofacies without a matrix), their sedimentary structure (i_3: *m* for massive, *x* for stratified), and complementary information in some instances (i_4: *o* for openframework (matrix-free lithofacies), *b* for a bimodal particle size distribution).

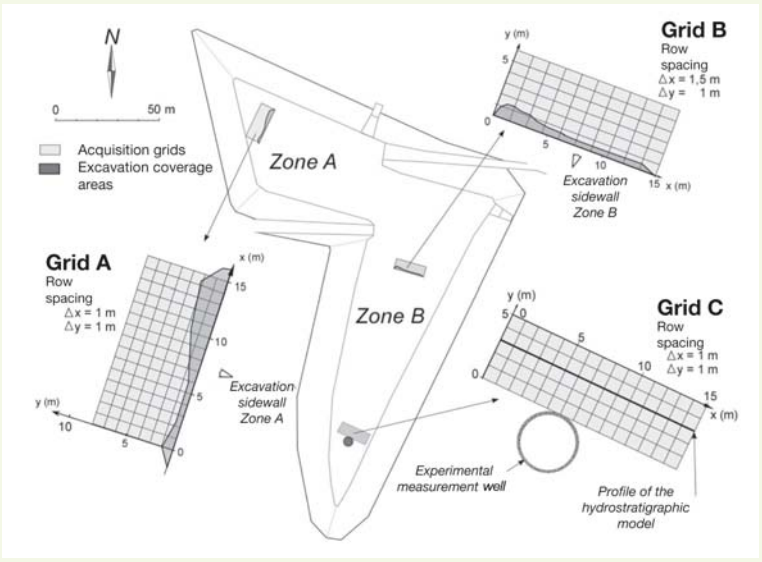

figure 2
Diagram of the DjR infiltration basin and location of acquisition grids A, B and C for the geophysical measurements. Grids A and B are both positioned in back of an excavation, in order to calibrate the geophysical signals with sedimentary heterogeneities. The coverage areas of excavations over the acquisition grids are depicted. On Grid C, the radar profile used to build the two-dimensional hydrostratigraphic model has also been represented

tableau 1
Classification code for alluvial lithofacies proposed by Miall **[22]** *and then extended by Heinz* et al. **[21]**. *This code entails juxtaposing indices of the type I_1 i_2 i_3 and i_4*

Index	Characteristics		Abbreviations
I_1	Predominant particle size distribution fraction		G: gravels S: sands
i_2	Texture	Gravel	c: clast-supported (granular support) m: matrix-supported (abundant matrix)
		Sands	-: no fine matrix within the sands
i_3	Sedimentary structure		x: stratified m: massive (no internal stratification) g: graded ranking (normal, inverse)
i_4	Complementary information		o: openframework b: bimodal

This code, employed in the field, was then completed in the laboratory by a grain size analysis. Dry sieving (Standard NF P94-056) was carried out on the 86 sampled lithofacies of Zone A. A wet sieving procedure according to Standard NF P18-560 (separation of the finest particles), followed by dry sieving, was conducted on each of the 41 samples extracted on the excavated sidewall of Zone B. The mean grain size and sorting of each grain size distribution curve were then determined using the Folk and Ward method **[23]**.

The grain size of the lithofacies described on the excavated sidewalls were compared with the glaciofluvial lithofacies located on the surface of recent glaciofluvial outwash plains, in order to evaluate the analogies between lithofacies having the same sedimentological classification code. The outwash plains studied herein were the proglacial zone of *the Bossons* Glacier (Chamonix, France), the sandur of the Breidamerkurjökull (Iceland) and the glacial and periglacial deposits of a quarry located in Saint-Cézaire (Quebec).

› Textural scale: Hydrofacies

Unsaturated flow modeling requires good knowledge of the hydraulic properties of each lithofacies input into the model. We use the term hydrofacies in order to refer to the hydrogeological units corresponding to the lithofacies for which a set of homogeneous hydraulic properties have been defined. The input data of unsaturated flow models are limited to the adjustment parameters of characteristic hydraulic curves models, i.e. water retention curve, which correlates capillary pressure with volumetric water content, as well as for the hydraulic conductivity curve, which correlates hydraulic conductivity with volumetric water content. These curves are often characterized in the laboratory on reworked samples. Only a few measurements are actually performed *in situ* and thus able to reflect field anisotropies. Moreover, laboratory measurements often prove infeasible for materials containing a predominant gravel fraction.

In this study, *in situ* hydraulic characterization tests were conducted both on glaciofluvial lithofacies accessible at the surface of glaciofluvial outwash plains analogous to the one at the east of Lyon during the last glacial maximum and mentioned above, and on the glaciofluvial lithofacies present at the DjR basin surface. The hypothesis is adopted here that two lithofacies with the same sedimentological classification code, i.e. similar in their genesis and texture, exhibit equivalent hydraulic properties. This hypothesis has also been formulated by Klingbeil **[24]** and Klingbeil *et al*. **[12]**, in order to assign to analogous lithofacies the hydraulic properties measured on Quaternary glaciofluvial lithofacies accessible to measurement. Klingbeil **[24]** furthermore demonstrated that the measured hydraulic properties are similar to those determined in equivalent sedimentary environments.

The method applied is known as BEST (for Beerkan Estimation of Soil Transfer parameters), as described by Lassabatère *et al.* **[25]**. This method involves single ring infiltration tests with at null pressure head, or Beerkan tests **[26,27]**. The BEST method is used for determining the shape and scale parameters of both the capillary retention h(θ) and hydraulic conductivity $K(\theta)$ curves, modeled respectively by the van Genuchten relation with the Burdine condition **(Equation 1)** and by the Brooks and Corey relation **(Equation 2)**:

$$\frac{\theta-\theta_r}{\theta_s-\theta_r}=\left[1+\left(\frac{h}{h_g}\right)^n\right]^{-m} \qquad m=1-\frac{2}{n} \tag{1}$$

$$\frac{K(\theta)}{K_s}=\left(\frac{\theta-\theta_r}{\theta_s-\theta_r}\right)^{\eta} \tag{2}$$

with:

θ: volumetric water content

h: capillary pressure

θ_s: saturated water content

θ_r: residual water content

K_s: saturated hydraulic conductivity

h_g: scale parameter of the water retention curve

m, *n* and η: shape parameters.

The residual water content θ_r is assumed to be zero. Parameters *m* and *n* are related by the Burdine condition. The two characteristic curves are thus fully described by 2 shape parameters (*m* or *n*, and η) and 3 scale parameters (h_g, K_s, θ_s).

The shape parameters, which depend primarily on sample texture **[28,29]**, are estimated based both on the grain size distribution of the fine fraction (< 2 mm) and on porosity of the studied lithofacies. In the case of coarser materials, the hypothesis is adopted of flow via the sandy and fine matrix. Scale parameters depend on the deposit structure and are determined by adjusting an experimental axisymmetrical infiltration curve on the analytical expression for 3D cumulative infiltration proposed by Haverkamp *et al*. **[30].** Details of the method and parameter estimation principle (using the BEST algorithm) have been presented by Lassabatère *et al*. **[25].**

The BEST method will be considered as having been validated for grain size fractions of less than 2 mm; this approach serves to ensure the presence of capillary phenomena, which predominate during the transient infiltration regime, and to fit the analytical expressions for cumulative infiltration to experimental data. When the BEST method cannot be validated (e.g. the case of coarse lithofacies with a negligible grain size fraction below 2 mm), the physico-empirical model developed by Arya and Paris **[31]** was introduced. This model linearly relates the grain size distribution of a sample to its pore size distribution, which may be estimated from the grain size distribution curve divided into a finite number *N* of size categories. The grain size fraction *i* ($1 \le i \le N$), defined by the number of particles N_i and average grain size R_i, gets associated with a volume of pores considered to be cylindrical and defined by radius r_i. Void index e is assumed to be identical for all grain size categories so defined. Arya and Paris **[31]** proposed the following relation, which serves to correlate each grain size R_i to a pore size r_i:

$$r_i=R_i.\left(\frac{2.e}{3}.N_i^{1-\alpha}\right)^{1/2} \tag{3}$$

where α is an empirical factor related to the tortuosity of the medium and set at a constant value of 1.38. The pore radius is then related with capillary pressure through Laplace's Law:

$$h_i = \frac{2.\gamma.\cos\Theta}{\rho_w.g.r_i} \quad (4)$$

where γ is the surface tension of water, Θ the contact angle, ρ_w the density of water and *g* gravitational acceleration.

The volumetric water content is then obtained by calculating the volume of water filling the pores associated with fractions *i*:

$$\theta = \sum_{j=1}^{i} \frac{\left(W_j / \rho_s\right).e}{V_{tot}} \quad (5)$$

where W_i is the mass of grain size category i, ρ_s corresponds to the particle density (assumed equal to 2.65 g.cm^{-3} given the sample mineralogy), and V_{tot} is the total volume defined by $V_{tot} = \rho b\, \Sigma W_i$ with ρ_b being the bulk density of a sample. This expression presumes that the pore volumes associated with each particle size category are gradually accumulated and filled with water, from the finest to the coarsest size category. Hydraulic conductivity is estimated using the Brooks and Corey model.

› Structural heterogeneities

The glaciofluvial deposits also display heterogeneity at the structural scale, as characterized by a variety of architectural elements. Each such element, or structural unit, is defined as an assembly of various lithofacies connected to one another by a single deposit phase (e.g. paleochannel filling); it is characterized by internal geometries and the external shape delimited by boundary surfaces like erosion surfaces **[21]**. The glaciofluvial structures were identified on the sidewalls of the two trenches cut in Zones A and B. An interpretation of the paleoenvironment has also been provided.

This sedimentological description was then compared with geophysical profiles measured vertically to the trench sidewalls prior to excavation. The main features of the geophysical signals were correlated with the interfaces between lithofacies and architectural element boundaries; the geophysical signals were thus calibrated on the structural units as well as on the glaciofluvial lithofacies. Geophysical profiles measured in back of the excavations enabled tracking the lateral evolution of geophysical signals; this evolution was correlated with the three-dimensional structure of the glaciofluvial architectural elements. A typology of geophysical signals valid at the local scale of the studied infiltration basin, in connection with both the textural and structural characteristics of the glaciofluvial deposit, was proposed. This typology was then used to interpret the glaciofluvial structures of a zone with an unknown sedimentary structure (i.e. absence of sedimentological description based on excavation).

The geophysical methods employed are Ground Penetrating Radar (GPR) and electrical resistivity. The GPR measurements were carried out with the GSSI SIR 3000 system (Geophysical Survey System Inc., Salem, U.S.A.) of the LRPC Autun, operated with a shielded antenna at a central frequency of 400 MHz, running in monostatic mode. The data processing was performed using the GSSI Radan 6 software. This processing consisted of a distance normalization, a static time shift (to align direct ground wave arrival to 0 ns), a background removal (to eliminate the high-amplitude direct ground wave), and a Kirchhoff migration. The electromagnetic wave velocity was determined by correlating characteristic radar reflectors with sedimentary interfaces characterized on the excavation sidewalls. This velocity ranged from 0.094 m.ns^{-1} to 0.111 m.ns^{-1}, with a mean value of 0.102 m.ns^{-1}. A velocity of 0.1 m.ns-1 was selected to convert two-way travel time into actual depth. This value is similar to velocities measured using the CMP method in the unsaturated zone of analogous Quaternary deposits **[4,7,32,33]**. As regards the electrical resistivity method, electrical profiles were measured using a Terrameter SAS 4000 in associa-

tion with the LUND multi-electrode system (ABEM, Mordelles, France). A 32-electrode, dipole-dipole method was also used, with a 1-m electrode spacing. The apparent resistivity profiles were obtained after signal inversion, performed with the Res2Dinv software.

The geophysical data were acquired on 3 acquisition grids **(see Fig. 2)**, positioned in back of the trench sidewall (Grids A and B) and on a third zone located at the northern periphery of the experimental measurement well (Grid C). The results obtained from Zone B have already been published **[34]** and therefore will not be presented herein. The dimensions of the Zone A acquisition grid were 15 m x 7 m, and the grid was oriented 18° N, parallel to the trench dug after the geophysical investigation. The spacing between each grid line was set at 1 m. Ground Penetrating Radar measurements were performed on all acquisition grid lines. For the electrical resistivity component, only the lines directed south-north were used for measurement purposes. As for Grid C, the GPR measurements were conducted on a 15 m x 6 m acquisition grid (with 1-m spacing between lines in each direction). The grid orientation was at 115°N. A single electrical resistivity profile was measured on the northern periphery of the acquisition grid.

› Modeling of unsaturated flows

To better demonstrate infiltration mechanisms in the heterogeneous unsaturated zone of the infiltration basin, an interpretative model of lithofacies and architectural element distribution for the glaciofluvial deposit was defined so as to perform the modeling of unsaturated flows. This model was elaborated by interpreting the geophysical signals measured on Grid C through implementation of the geophysical signal typology. The 2D profile used to build the model has been chosen so that it orthogonally cuts the longest continuous direction of a fluvioglacial architectural element. These directions were determined by adjusting a linear anisotropic model on the experimental variogram of depths at each interface between architectural elements. The selected 2D profile is depicted on **Figure 2**. The modeling conducted based on this interpretative model may be compared with experimental measurements of water content variations (via the experimental measurement well shown on **Fig. 2**, instrumented with TDR probes). These experimental measurements have not been included in this article. The objective here has simply been to illustrate the effect of sedimentary heterogeneity on flows within the unsaturated zone of the DjR basin.

The hydrostratigraphic model has been incorporated into the Hydrus2D software **[35]**, thereby allowing for the numerical modeling of two-dimensional flows in both unsaturated and saturated media (with numerical solutions of Richards' Equation obtained using the finite element method). A scenario corresponding to the infiltration of an 11-cm water layer during one hour under initial high humidity conditions was modeled; this scenario corresponds to a rainfall event subsequent to another recent rainfall event.

With respect to hydraulic properties, the Hydrus2D application input data correspond to the van Genuchten model parameters with the Mualem condition (m = 1-1/n), which differs from the conditions determined by the BEST method. To generate appropriate input data, an adjustment of parameters m and n, as determined by the BEST method and the Arya and Paris model, was undertaken using the RETC software **[36]**. RETC was also applied to adjust the residual water content θ_r, assumed to equal zero during estimation of the scale parameters and taken into account during modeling so as to yield more realistic input data.

As for the selected boundary conditions, a free drainage condition was set at the lower model boundary. The lateral boundaries were taken as seepage faces, in order to circumvent an unrealistic water accumulation at the border of the domain, through allowing lateral flows in the case of deposit saturation at the domain boundary. Furthermore, the flows were mainly studied over the central part of the domain, in the aim of limiting the influence of the seepage condition on both the water content and capillary pressure values. On the surface, a constant evaporation rate of 2.6 mm.d^{-1} was imposed during an initial 250-minute drainage phase; these initial condi-

tions correspond with a complete saturation of the medium. The next phase spanned a 60-minute period of infiltration. A boundary condition corresponding to a constant 11-cm hydraulic head was adopted. During a final drainage phase, a constant evaporation rate of 2.6 mm.d^{-1} was once again imposed.

RESULTS AND DISCUSSION

Characterization of the sedimentary and hydraulic heterogeneities at the textural scale

› Typology of the glaciofluvial deposit lithofacies underlying the DjR basin

The textural heterogeneity of the glaciofluvial deposit is reflected by the presence of four distinct lithofacies **(see Table 2)**: medium sands (S-x lithofacies), sand and gravel mixes, with a dominant heterometric gravel fraction (Gcm lithofacies) or with a bimodal grain size distribution (Gcm,b lithofacies), and gravel without any sandy or fine matrix (Gcx,o and Gcg,o lithofacies). The sand and gravel mixes (Gcm and Gcm,b lithofacies) constitute the predominant lithofacies of the glaciofluvial deposit. Goutaland *et al*. provided a sedimentological interpretation of each lithofacies **[34]**. The sands are low-flow regime deposits, whereas the Gcm lithofacies corresponds to a high flow stage deposit. The Gcm,b and Gcg,o lithofacies formed by gravel dunes migration and Gcx,o lithofacies resulted from gravel bars migration. The Gcg,o and Gcm,b lithofacies are often associated with one another. Their alternation yields a structure already widely described in the literature on glaciofluvial deposits, via the term *gravel couplets* **[37,38]** *or alternating gravel* **[21]**.

The entire set of lithofacies sampled on the sidewalls of both excavations dug into the DjR basin were depicted on a gravel/sands/fines triangular diagram **(see Fig. 3)** (featuring 117 samples in all, including 16 S-x lithofacies, 28 Gcx,o or Gcg,o lithofacies, 38 Gcm lithofacies and 35 Gcm,b lithofacies). The domains relative to the four types of lithofacies could thus be defined. The Gcg,o and Gcx,o lithofacies display a gravel fraction in excess of 90%, while the Gcm and Gcm,b lithofacies contain between 70% and 90% gravel. The S-x lithofacies exhibit a sand fraction above 70% and a fines fraction of less than 5%. The limit between Gcm and Gcm,b lithofacies lies roughly at a 15% sand fraction.

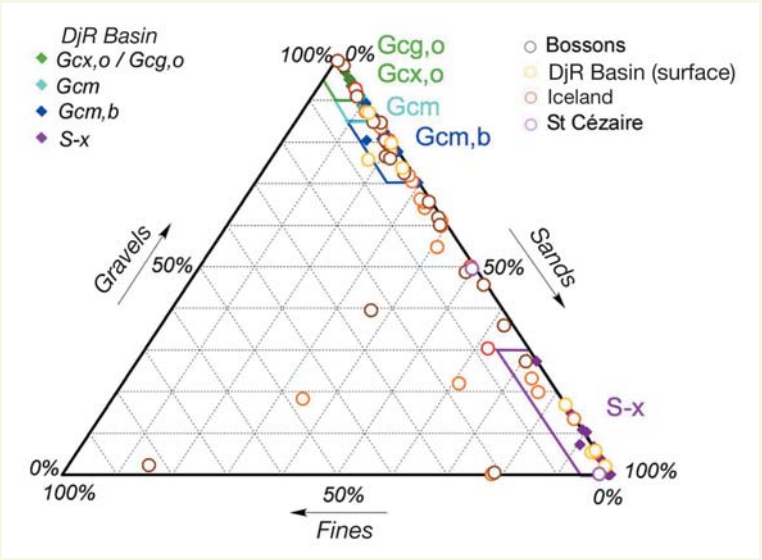

figure 3
Textural triangle representing the fractions of gravels (D > 2 mm), sands (2 mm > D > 63 µm) and fines (clays and silts, D < 63 µm) of the glaciofluvial lithofacies underlying the DjR basin, as well as the lithofacies of the Bossons glacier, proglacial zone, the Breidamerkurjökull glaciofluvial outwash in Iceland and the Saint-Cézaire Quaternary formations in Quebec

Lithofacies		Grain size distribution
Photograph	Lithology	
Facies 1: S-x		
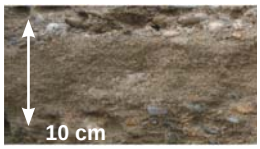	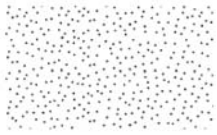	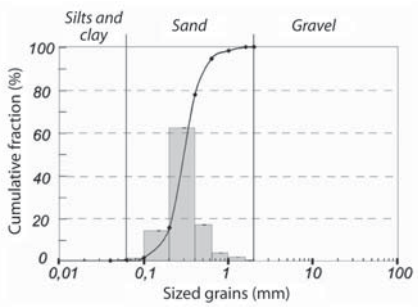
Medium sands, poorly to moderately well sorted, with a mean grain size of 325 ± 43 µm, without any silty or clayey matrix, internal planar or inclined laminations corresponding to the sand sedimentation phases		
Facies 2: Gcm		
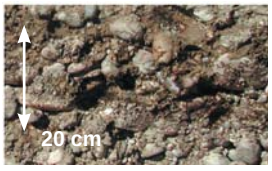	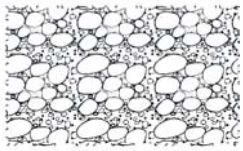	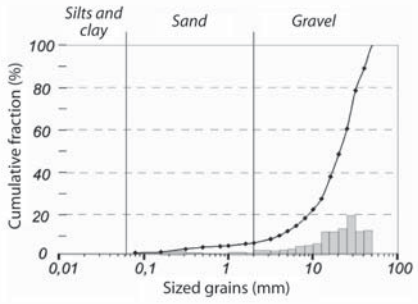
Sand and gravel mixes displaying a heterometric grain size distribution (from fine sands to coarse gravels), typically present in the first 30 centimeters underneath the basin surface, with the gravel fraction being dominant (85%)		
Facies 3: Gcm,b		
	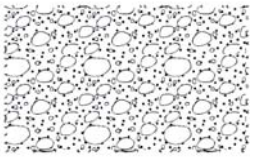	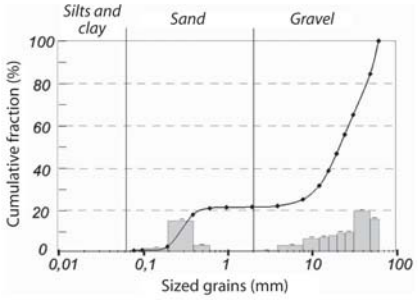
Sand and gravel mixes with a bimodal grain size distribution, featuring a coarse mode (medium to coarse gravel) and a sandy mode (matrix of medium sands with a mean grain size of 325 µm)		
Facies 4: Gcx,o/Gcg,o		
	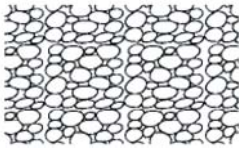	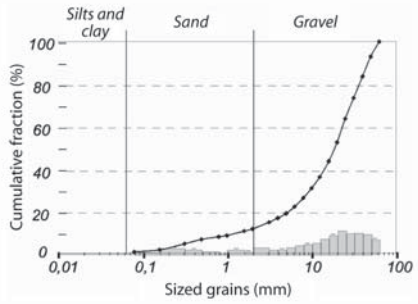
Poorly to moderately well sorted matrix-free gravel, in the centimeter size range for the coarsest elements, in the form of prograding inclined lenses (Gcg,o) or thin subhorizontal layers (Gcx,o)		

tableau 2
Typology of glaciofluvial deposit lithofacies underlying the DjR basin. The classification code used is the same as in **Table 1**. *The glaciofluvial deposit is primarily composed of the Gcm and Gcm,b lithofacies*

Figure 3 also shows the lithofacies characterized on the surface of the DjR basin along with recent glaciofluvial outwash plains (a total of 57 samples, including 17 S-x lithofacies, 3 Gcx,o lithofacies, 24 Gcm lithofacies and 10 Gcm,b lithofacies). In all, 33 of the 57 recent lithofacies examined exhibit grain size fractions in gravel/sands/fines corresponding with the size distribution criteria stated above for the four types of lithofacies. Glaciofluvial lithofacies analogous to those described in **Table 2** are thus present on the recent glaciofluvial outwash plains, which confirms the hypothesis accepted among sedimentologists that studying recent analogous formations serves to understand the heterogeneity of an older deposit. Similar genetic processes lead to the formation of recent similar lithofacies in terms of grain size distribution at the former Quaternary lithofa-

cies, having the same sedimentological code. A comparison of the recent and former lithofacies however shows that for the same sedimentological classification code, the grain size fractions in gravel/sands/fines are highly variable and may deviate from the values expected based on the criteria defined above. Due to the accessibility of surface lithofacies, recent glaciofluvial outwash plains constitute preferential zones for conducting *in situ* hydraulic characterization tests.

› Definition of glaciofluvial hydrofacies

An evaluation of hydraulic properties was undertaken on the 33 recent analogous lithofacies with grain size fractions similar to those of the glaciofluvial lithofacies from eastern Lyon.

The saturated hydraulic conductivities estimated from the BEST method were then compared with the values estimated using the Kozeny-Carman model (Chapuis and Aubertin expression **[39]**) applied on the lithofacies of **Table 2** and on values taken from the literature **[12,21,33,38,40,41].** The result is presented in **Figure 4**.

The Kozeny-Carman expression yields an acceptable value of saturated hydraulic conductivity for the S-x and Gcx,o lithofacies compared to values from the literature. In contrast, estimated values for the Gcm and Gcm,b lithofacies have been overestimated.

As regards values derived from the bibliography, the saturated hydraulic conductivity varies over several orders of magnitude, reflecting hydraulic heterogeneity within hydrofacies of the same classification code. Only the saturated hydraulic conductivity from the Gcx,o lithofacies is significantly different from the other lithofacies.

Figure 4 indicates a strong level of agreement between the values estimated by BEST and those stemming from the literature for sandy lithofacies (S-x) or lithofacies with a sandy matrix (Gcm and Gcm,b). This comparison makes it possible to validate the BEST algorithm for estimating the saturated hydraulic conductivity of lithofacies containing a high sand fraction in matrix form or as the predominant fraction. For the numerical modeling of flows, the hydraulic properties of a lithofacies for each of the S-x, Gcm and Gcm,b types, as estimated using the BEST method, were selected. The residual water content, presumed to equal zero during the shape parameter estimation, was adjusted using the RETC application. **Figure 5** shows the water retention and hydraulic conductivity curves of the target lithofacies, and **Table 3** summarizes the shape and scale parameters of these curves. The water retention curve for the Gcm,b lithofacies does not follow a bimodal pattern since the BEST method estimation is applied to the grain size fraction below 2 mm of this lithofacies, which is equivalent to adopting the hypothesis of a flow by the matrix fraction of this lithofacies

figure 4
Comparison of the estimations of saturated hydraulic conductivity for hydrofacies S-x, Gcx,o, Gcm and Gcm,b using the BEST method and Kozeny-Carman relation with values found in the literature

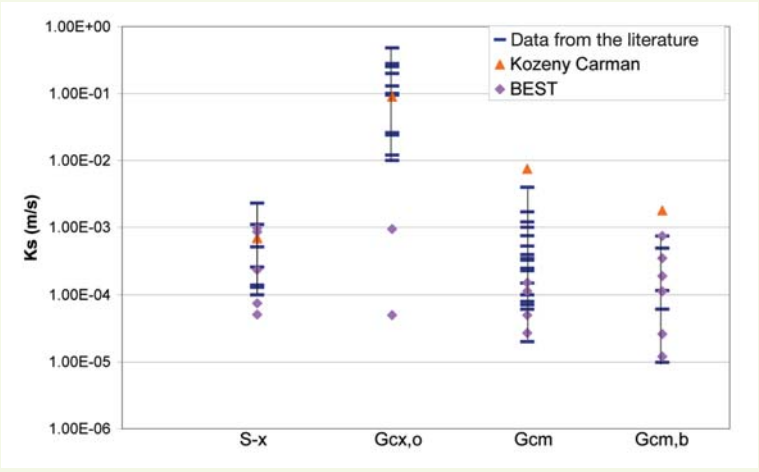

figure 5
Capillary pressure h (a) curves and hydraulic conductivity K (b) curves vs. volumetric water content θ for the four types of glaciofluvial lithofacies present underneath the DjR basin

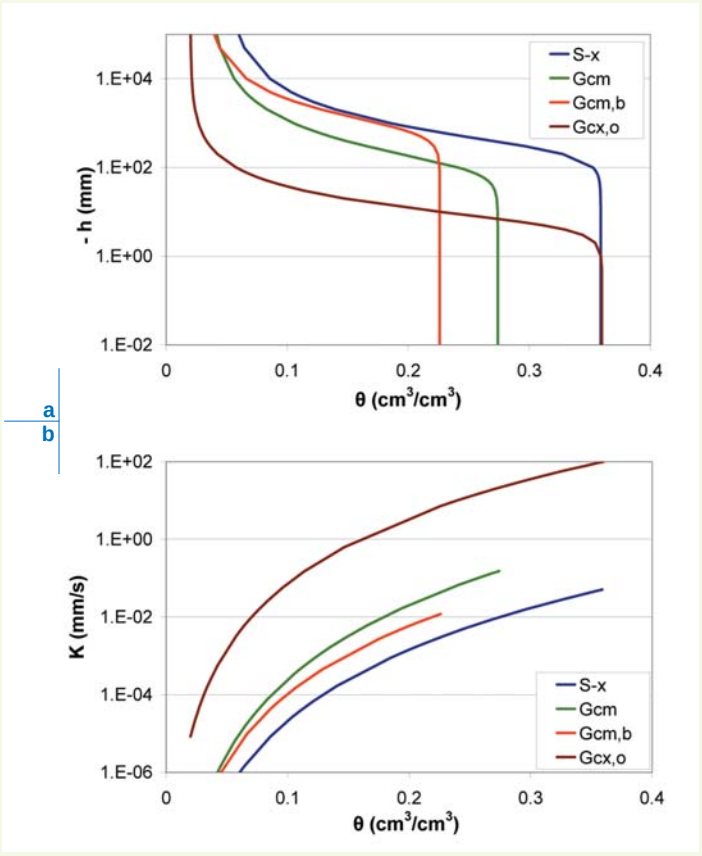

tableau 3
Shape (n) and scale (θ_r, θ_s, h_g and Ks) parameters used in modeling unsaturated flows with Hydrus2D

Lithofacies	θ_r	θ_s	h_g (m)	n	K_s (m.s^{-1})
Gcm	0.036	0.274	0.211	2.4	$1.53.10^{-4}$
S-x	0.051	0.359	0.450	2.61	$5.10.10^{-5}$
Gcx,o / Gcg,o	0.02	0.36	0.009	2.7	$1.00.10^{-1}$
Gcm,b	0.032	0.226	1.190	2.71	$1,20.10^{-5}$

Regarding the Gcx,o lithofacies, the saturated hydraulic conductivity value has been underestimated in comparison with values found in the literature. Saturated hydraulic conductivities have been estimated at values less than 10^{-3} m.s^{-1}, whereas values stemming from the literature lie above 10^{-2} m.s^{-1}. This underestimation may be explained by the inappropriateness of the BEST method for this type of lithofacies, which exhibits merely a very small sand and fine fraction **(Table 2)**. A characterization of the hydraulic properties of this lithofacies was thus obtained from the Arya and Paris model for the representative analogue of the proglacial zone of the Bossons glacier. The saturated hydraulic conductivity as well as porosity were determined based on values furnished from the bibliography **[12]**. Adjustment of the van Genuchten function with a Mualem condition shows a good level of correlation with the data estimated from the Arya and Paris model ($r^2 = 0.996$). The characteristic hydraulic curves relative to the Gcx,o lithofacies have been depicted on **Figure 5**, while the associated shape and scale parameters are listed in **Table 3**. The air entry pressure, which corresponds to the capillary pressure at which the lithofacies transition from a saturated state to a partially-saturated state, lies on the order of -2 mm, i.e. 25 to 200 times less than the air entry pressure of the sandy lithofacies or lithofacies with a sandy matrix. This low air entry pressure is compatible with the macroporous structure of the lithofacies

Characterization of the structural configuration and calibration of the geophysical signals

› Structural characterization of the glaciofluvial deposit

The structural heterogeneity is related to the paleo-environments of the deposit. An interpretation of these environments serves to understand the overall organization of the lithofacies.

Two distinct levels were revealed over the first three meters of the glaciofluvial deposit underlying the DjR basin **(Fig. 6)**:

– a lower level (located at depths greater than 0.5 m on average) corresponding to a braided proglacial system deposit, leading to structures as paleochannel and scour fill (S-x, Gcx,o, Gcm and Gcm,b lithofacies), and gravel progradations (Gcx,o and Gcm,b lithofacies). This level comprises structural units 1, 2 and 3 of the sidewall of Zone A and units 5 and 6 of the sidewall of Zone B;
– an upper level (on average located above a depth of 0.5 m) corresponding to a deposit at a high stream energy, which lies at the origin of the presence of a very heterometric sand and gravel mix (Gcm lithofacies). This level comprises structural units 4 and 7 on the sidewalls of Zones A and B, respectively.

The braided proglacial channel environments have been widely described in the literature, especially in the Rhine River glaciofluvial alluvia **[9,12,21,37,38].** The glaciofluvial deposits of eastern Lyon were set in an analogous environment.

The presence of a similar upper level between the two study zones leads to the hypothesis of an allocyclic event at the basin scale. It could be a phase of flooding in the glaciofluvial outwash, at the origin of the erosion surface present at the base of units 4 and 7 and by the heterometric grain size distribution composing these units.

figure 6
Delimitation of the structural units and primary lithofacies of the excavation sidewalls created in Zones A (a) and B (b)

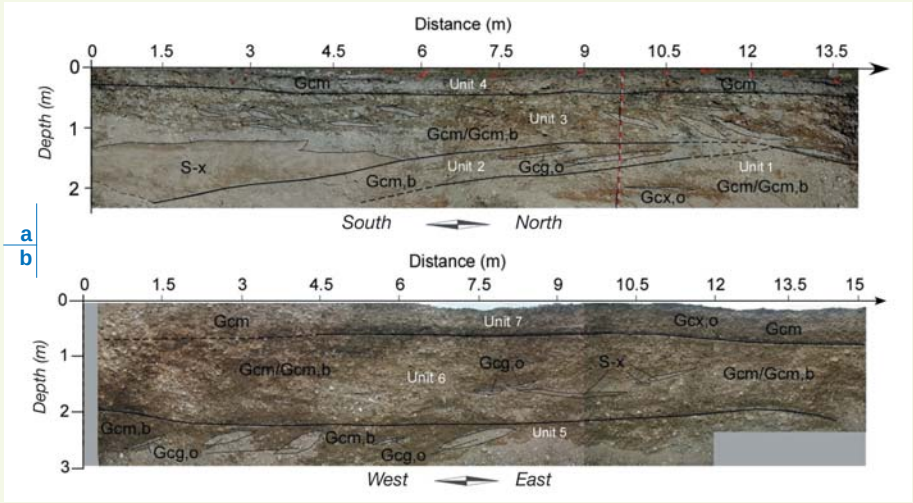

› Typology of the geophysical signals

Figure 7 summarizes the main stratigraphic characteristics of the Zone A excavation sidewall, along with the corresponding GPR and resistivity profiles. The investigation depth equals 3 m with the GPR and 4.6 m with electrical resistivity. Unit 1 corresponds to continuous and parallel radar reflectors dipping towards the north. The resistivities in this unit vary between 1,000 and 1,400 Ω.m. This unit pertains to the unsaturated sand and gravel mix with a dominant gravel fraction. Unit 2 is relatively fine and corresponds to high-amplitude and sub-parallel radar reflectors, dipping southward. This structure is not clearly identifiable on the resistivity profile, even though

resistivity values remain high (1,000 Ω.m). These geophysical characteristics are correlated with the fine matrix-free gravel layers observed on the excavation sidewall. Unit 3 is characterized by inclined reflectors dipping northward, as well as curved reflectors at depths of between 1 and 2 m. The upper part of Unit 3 features high-amplitude, sub-parallel radar reflectors dipping northward. The curved shape oriented upward can be observed on the resistivity profile where resistivity is decreasing with variations of between 500 and 1,000 Ω.m. This decrease corresponds to a change in lithology (sandy lenses). The upper unit (Unit 4) features continuous, sub-horizontal and high-amplitude reflectors. Resistivities over the first meter of depth are rather low (between 200 and 500 Ω.m). Due to proximity of the basin surface, this unit contains a higher quantity of fine particles (silts and clays) **[42]**, which leads to a higher water content and explains the accentuation in high-amplitude radar reflectors close to the surface, along with low resistivity values. At depths of between 3 and 4.6 m, where only resistivity data are available, the high-resistivity lobe underneath Units 2 and 3 (between $x = 2$ m and $x = 7$ m) is interpreted by the presence of a greater quantity of coarse gravel. This calibration shows that the main structural and textural characteristics described on the excavation sidewall are indeed characterized by the two geophysical methods: ground penetrating radar and electrical resistivity are complementary, although radar reflectors provide details more easily correlated with stratigraphic units (in particular the inclination of stratigraphic unit).

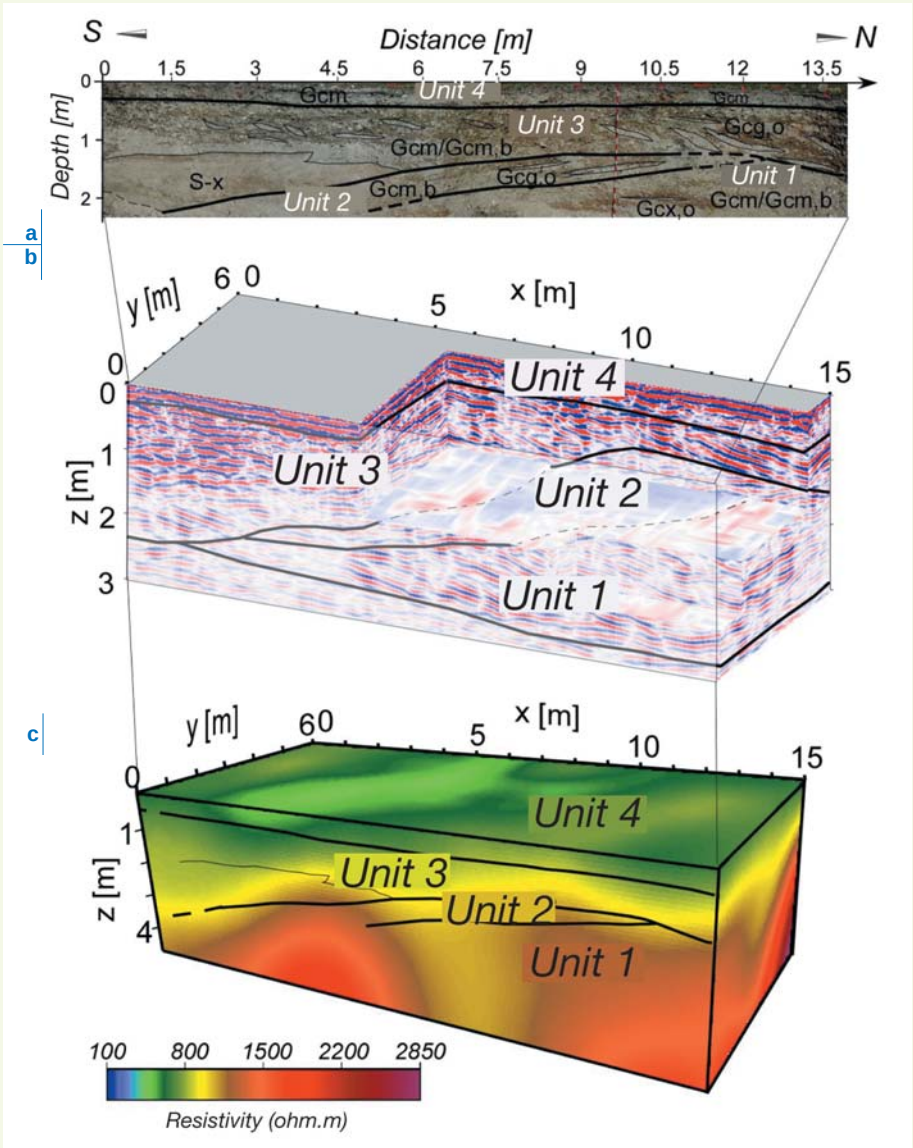

figure 7
Cross-referenced interpretation of the excavation sidewall for Zone A (a) decomposed into structural units and lithofacies **(table 2)**, *and corresponding geophysical investigations using geological radar (b) and electrical resistivity (c)*

The various geophysical characteristics highlighted above were then correlated with the sedimentological description generated at both the structural and textural scales. A typology of three geophysical facies relating geophysical characteristics with sedimentary structures could thus be defined **(Table 4)**. Radar reflectors are simpler to connect with sedimentary structures than apparent electrical resistivities. Since electrical resistivity is extremely sensitive to water content variations (electrical resistivities vary from 100 Ω.m in saturated gravel to 1,400 Ω.m in dry gravel), no standard resistivities have been proposed in this typology. Only the observations on qualitative resistivity variations have been included.

tableau 4
Typology of radar reflectors and electrical resistivity characteristics relative to lithofacies organization, deposit elements and associated paleoenvironment

Geophysical characteristics			Sedimentary characteristics
GPR reflectors		Electrical resistivity	- Associated lithofacies - External shape of architectural elements - Associated paleoenvironment
Reflectors	Internal structure		
 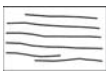 High-amplitude, subhorizontal or slightly inclined, continuous and parallel		Low resistivity (high water content correlated with a greater quantity of fine particles)	- Gcm; higher fine particle fraction (silts and clays) - subhorizontal or inclined plane - Flooding phase in the outwash plain
  Short, wavy or curved		Local decrease in resistivity (higher sand fraction)	- Primarily Gcm or Gcm,b; presence of sandy lens (S-x) - Channel shape - Filling of scours or channels in the outwash plain
 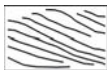 Relatively high amplitude, oblique, continuous, sub-parallel, sometimes short and curved		Local increase in resistivity (macropore desaturation, higher gravel fraction)	- Progradation of Gcg,o / Gcm,b lithofacies - Concave shape - Filling of scours or channels in the outwash plain

Modeling of unsaturated flows

› Definition of a glaciofluvial hydrostratigraphic model

In order to illustrate the role of both the textural and structural sedimentary heterogeneities of the glaciofluvial deposit on flows in the unsaturated zone of the DjR basin, a two-dimensional hydrostratigraphic model was built according to interpretation of the geophysical data acquired at the level of Grid C **(see Fig. 2)**, by implementing the typology defined in **Table 4.** Four primary units were highlighted and have been designated Units 8 through 11 in order of decreasing depth **(Fig. 8).** The hydraulic properties determined above were assigned to the lithofacies of this model, so as to establish a hydrofacies distribution model for application to modeling unsaturated flows. This step was performed by use of the Hydrus2D software within a domain covering a reduced zone 4.5 m wide and 3 m deep, as demarcated on **Figure 8**. This zone offers the advantage of combining all the hydrofacies characterized in the studied glaciofluvial deposit. Discretization (18,000 triangular mesh elements) was carried out so as to obtain the best compromise between computation time and level of precision in model results.

› Results from modeling exercise

Figure 9 displays the evolution in both the volumetric water content field and capillary pressure of the hydrostratigraphic model subsequent to a constant infiltration flow lasting 60 min (between T = 0 and T = 60 min).

The initial water content field serves to highlight the link existing between sedimentary heterogeneity and hydraulic heterogeneity. The matrix-free gravel hydrofacies are initially desaturated.

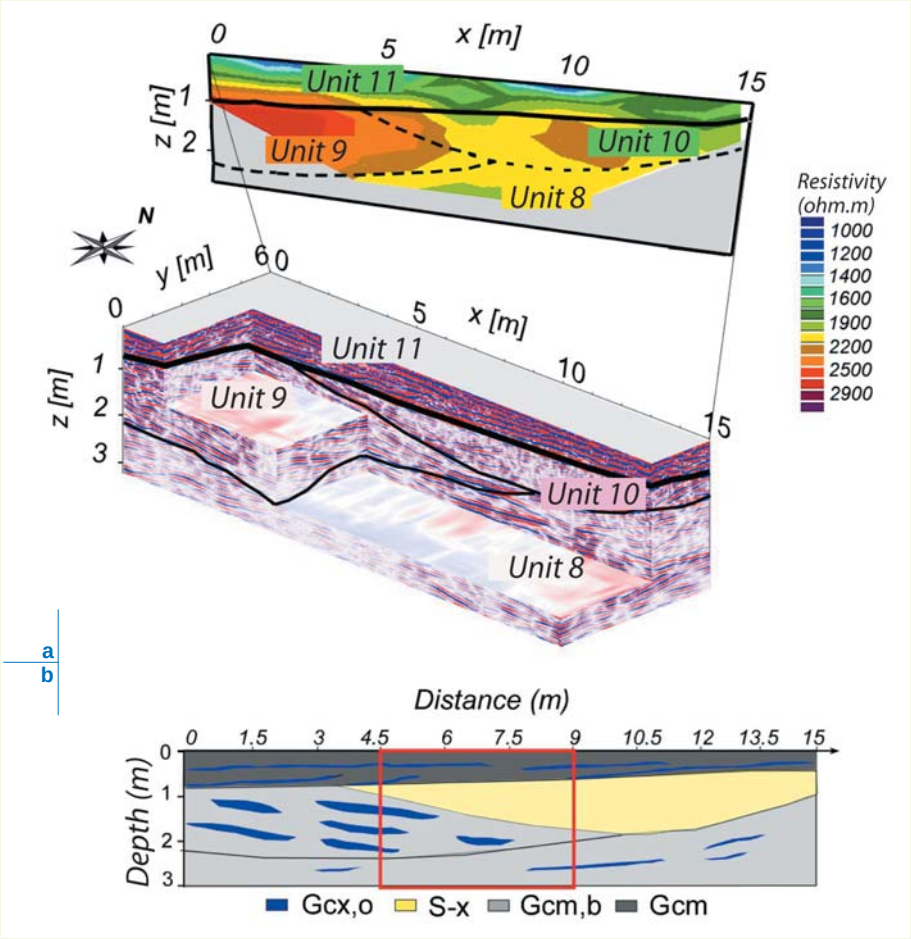

figure 8

- a: pseudo-3D block of radar profiles and resistivity profile corresponding with Grid C acquisition;
- b: the associated two-dimensional interpretative hydrostratigraphic model. Model orientation corresponds with a direction perpendicular to that of Unit 10 (glaciofluvial paleo-channel assumed to be filled solely by the S-x lithofacies). The delimitation in red on the hydrostratigraphic model corresponds with the domain boundaries selected for modeling with the Hydrus2D software package

Capillary barrier phenomena may be observed in the upper part of these hydrofacies (with water content locally higher above the Gcx,o lithofacies in Unit 11). The lowest capillary pressures are observed over the lower part of the Gcg,o lithofacies in Unit 9. This pressure is due to a fast drainage of the gravel layers, causing capillary barrier effects in their upper part and thereby limiting water flow heading towards their lower part. Moreover, the difference in hydraulic properties between Unit 10, composed of sandy hydrofacies, and the bimodal hydrofacies of the lower unit (Unit 8) leads to a local increase in water content at the level of the lower limit of Unit 10. Structural heterogeneities therefore induce heterogeneity in the water content field.

During infiltration (T = 20 min and T = 50 min), a rise in capillary pressure is observed within the sandy hydrofacies over its upper part at first, and then throughout Unit 10. This rise in turn causes a gradual saturation of Unit 10. The Gcx,o hydrofacies of Unit 11 gradually gets saturated after an increase in capillary pressure. At T = 50 min, the Gcg,o hydrofacies of Unit 9 also display an entirely saturated part. The strong hydraulic conductivity of these hydrofacies under water saturated or quasi-saturated conditions induces a rapid and essentially gravity flow within these layers.

Furthermore, two hours after infiltration has ceased (T = 180 min), the highest capillary pressures are located at the bottom of the flow zone. The drop in capillary pressure at shallow depths (Unit 11) causes a desaturation of Gcx,o hydrofacies. Capillary barrier effects thus appear at the interface of the Gcm and Gcx,o hydrofacies. The sandy hydrofacies retain a water content value near that saturated water content. The high capillary pressure values within Unit 9 explain the fact that the matrix-free gravel hydrofacies remains saturated for a long time after infiltration has ended.

figure 9

Evolution in both the volumetric water content and capillary pressure fields during the infiltration phase lasting 60 min (T = 20 min and T = 50 min) and during the consecutive drainage phase (T = 180 min, i.e. 120 min after the end of infiltration)

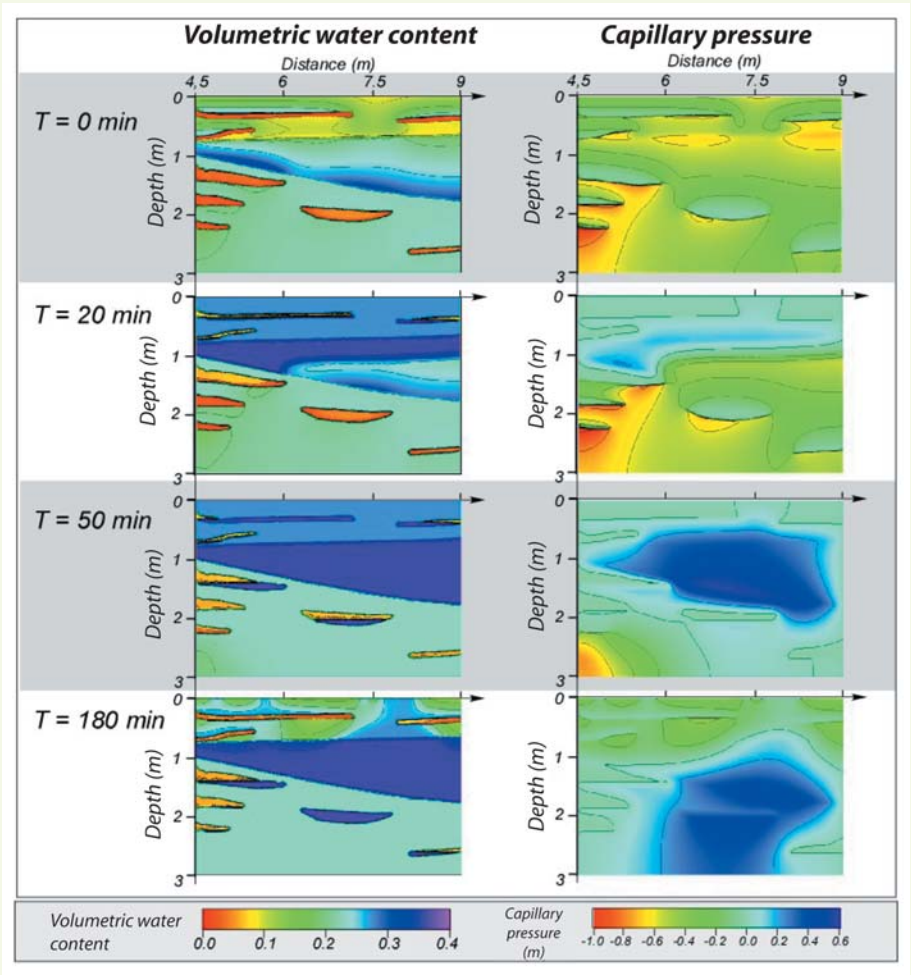

› Discussion

The results of this modeling exercise serve to assess the types of sedimentary heterogeneities lying at the origin of the heterogeneous distribution of the water content field or of preferential flow paths during infiltration.

Due to their high saturated hydraulic conductivity, the matrix-free gravel hydrofacies can act, in the case of complete water saturation, like preferential flow paths, which may remain activated for a long time after infiltration has ceased. The flows generated are rapid and essentially gravity-based; they therefore follow the most pronounced dip of these units. Two-dimensional modeling does not enable incorporating the actual three-dimensional flows arising in the case of saturation of these hydrofacies. The study of heterogeneous subsoils thus necessitates an understanding of the spatial distribution of sedimentary heterogeneities in three dimensions **[21]**.

These hydrofacies also exert an impact on the heterogeneity of the water content field under slightly saturated conditions, as they induce capillary barrier effects that engender a high capillary pressure gradient between their lower and upper parts. These capillary barrier effects may generate water accumulation in the lithofacies overlying matrix-free gravel **[43]**; they lead to lateral flow patterns, known as funneled flows **[13,15-17]**, giving rise to flow along the interface between a sandy lithofacies or a lithofacies with a sandy matrix and the matrix-free gravel.

Lastly, the interfaces between structural units also induce heterogeneity in the water content field. Knowledge of the geometry (orientation, dip) at the structural scale is therefore a prerequisite for evaluating the preferential flow paths

CONCLUSION

The results presented herein have focused on the role of sedimentary heterogeneities with respect to water flows within a part the unsaturated zone underlying an infiltration basin. The hydrogeophysical approach described allows evaluating the distribution of hydrostratigraphic units at the hydrofacies scale. The modeling of unsaturated flows underlying a stormwater infiltration structure must be conducted at this scale, as long as the hydrofacies can constitute preferential flow paths. Knowledge of the spatial distribution of hydrofacies in three dimensions nonetheless proves necessary in characterizing actual three-dimensional flows. Three-dimensional modeling efforts are currently underway.

The hydrogeophysical approach elaborated, which implements the principles of sedimentology, hydrodynamics in porous media and subsurface geophysics, may be used on other infiltration structures in order to obtain a realistic image, at the scale of these facilities, of the three-dimensional distribution of hydrostratigraphic units. The numerical modeling of flows based on this distribution must be three-dimensional, so as to incorporate the lateral flows (funneled flows) generated by interfaces between two different units. The coupling of hydrostratigraphic characterization with three-dimensional numerical modeling will then enable improving the understanding of unsaturated flows underlying infiltration structures; moreover by coupling the hydraulic data obtained with contaminant transfer mechanisms, it is possible to evaluate the risk of pollutants migrating at depths.

The model exhibited as part of this work still needs to be validated however. Experimental data on water content and capillary pressure variations subsequent to propagation of an infiltration front, as measured from the measurement well located in Zone C of the DjR basin, will be compared with values output by the model

ACKNOWLEDGEMENTS

The authors thank the French national research programs "ACI Ecosphere Continentale : EMMAUS" and "ANR Écotechnologie et Développement Durable : ECCOPLUIE" for the financial support, and the research federation O.T.H.U. for the technical support.

REFERENCES

1 **Galloway W. E.**, **Sharp J. M.**, *Characterizing aquifer heterogeneity within terrigeneous clastic depositional systems*. In : G. S. Fraser and J. Matthew Davis (Ed), Hydrogeologic Models of Sedimentary Aquifers, SEPM (Society for Sedimentary Geology), **1998**, pp. 85-90.

2 **Anderson M. P.**, Hydrogeologic facies models to delineate large-scale spatial trends in glacial and glaciofluvial sediments, *Geological Society of America Bulletin*, **1989**, vol. **101**, pp. 501-511.

3 **Huggenberger P.**, **Meier E.**, **Pugin A.**, Ground-probing radar as a tool for heterogeneity estimation in gravel deposits : advances in data-processing and facies analysis, *Journal of Applied Geophysics*, **1994**, vol. **31**, pp. 171-184.

4 **Beres M.**, **Huggenberger P.**, **Green A. G.**, **Horstmeyer H.**, Using two- and three-dimensional georadar methods to characterize glaciofluvial architecture, *Sedimentary Geology*, **1999**, vol. **129**, n° **1-2**, pp. 1-24.

5 **Huggenberger P.**, **Aigner T.**, Introduction to the special issue on aquifer-sedimentology : problems, perspectives and modern approaches, *Sedimentary Geology*, **1999**, vol. **129**, n° **3-4**, pp. 179-186.

6 **Asprion U.**, **Aigner T.**, Towards realistic aquifer models : three-dimensional georadar surveys of Quaternary gravel deltas (Singen Basin, SW Germany), *Sedimentary Geology*, **1999**, vol. **129**, n° **3-4**, pp. 281-297.

7 **Heinz J.**, **Aigner T.**, *Three-dimensional GPR analysis of various Quaternary gravel-bed braided river deposits (southwestern Germany)*. In : C. S. Bristow and H. M. Jol (Ed), Ground Penetrating Radar in Sediments, Geological Society of London, **2003**, pp. 99-110.

8 **Lunt I. A.**, **Bridge J. S.**, **Tye R. S.**, *Development of a 3-D depositional model of braided-river gravels and sands to improve aquifer characterization.* In : J. S. Bridge and D. W. Hyndman (Ed), Aquifer characterization, SEPM (Society for Sedimentary Geology), **2004**, vol. **80**, pp. 139-169.

9 **Huggenberger P.**, **Regli C.**, *A sedimentological model to characterize braided river deposits for hydrogeological applications*. In : G. H. Sambrook-Smith, J. L. Best, C. S. Bristow and G. E. Petts (Ed), Braided Rivers : Process, Deposits, Ecology and Management., Blackwell Publishing, **2006**, pp. 51-74.

10 **Winiarski T.**, **Crosnier J.**, **Vacherie S.**, **Métral B.**, Évaluation de la teneur en eau de la zone non-saturée d'un bassin d'infiltration de l'Est de Lyon

(France), *Novatech'2004*, Lyon, France, **2004**, vol. **2**, pp. 1541-1548.

11 **Winiarski T.**, **Bedell J.-P.**, **Delolme C.**, **Perrodin Y.**, The impact of stormwater on a soil profile in an infiltration basin, *Hydrogeology Journal*, **2006**, vol. **14**, pp. 1244-1251.

12 **Klingbeil R.**, **Kleineidam S.**, **Asprion U.**, **Aigner T.**, **Teutsch G.**, Relating lithofacies to hydrofacies : outcrop-based hydrogeological characterisation of Quaternary gravel deposits, *Sedimentary Geology*, **1999**, vol. **129**, nº **3-4**, pp. 299-310.

13 **Walter M. T.**, **Kim J.-S.**, **Steenhuis T. S.**, **Parlange J.-Y.**, **Heilig A.**, **Braddock R. D.**, **SelkerJ. S.**, **Boll J.**, Funneled flow mechanisms in a sloping layered soil : laboratory investigation, *Water Resources Research*, **2000**, vol. **36**, nº **4**, pp. 841-849.

14 **Hill D. E.**, **Parlange J. Y.**, Wetting front instability in layered soils, *Soil Science Society of America Proceedings*, **1972**, vol. **36**, nº **5**, pp. 697-702.

15 **Miyasaki T.**, Water flow in unsaturated soil layered slopes, *Journal of Hydrology*, **1988**, vol. **102**, pp. 201-214.

16 **Kung K.-J. S.**, Preferential flow in a sandy vadose zone, 2, mechanisms and implications, *Geoderma*, **1990**, vol. **46**, pp. 59-71.

17 **Heilig A.**, **Steenhuis T. S.**, **Walter M. T.**, **Herbert S. J.**, Funneled flow mechanisms in layered soil : field investigations, *Journal of Hydrology*, **2003**, vol. **279**, pp. 210-223.

18 **Heinz J.**, **Aigner T.**, Hierarchical dynamic stratigraphy in various Quaternary gravel deposits, Rhine glacier area (SW Germany) : implications for hydrostratigraphy, *International Journal of Earth Sciences*, **2003**, vol. **92**, pp. 923-938.

19 **BURGEAP**, Étude de la nappe de l'Est lyonnais, *Lyon*, **1995**, 45 pages + 11 cartes.

20 **Barraud S.**, **Gibert J.**, **Winiarski T.**, **Bertrand Krajewski J.-L.**, Implementation of a monitoring system to measure impact of stormwater runoff infiltration, *Water Science and Technology*, **2002**, vol. **45**, nº **3**, pp. 203-210.

21 **Heinz J.**, **Kleineidam S.**, **Teutsch G.**, **Aigner T.**, Heterogeneity patterns of Quaternary glaciofluvial gravel bodies (SW-Germany) : application to hydrogeology, *Sedimentary Geology*, **2003**, vol. **158**, nº **1-2**, pp. 1-23.

22 **Miall A. D.**, *Lithofacies types and vertical profile models in braided river deposits : a summary*. In : A. D. Miall (Ed), Fluvial Sedimentology, **1978**, vol. **5**, pp. 597-604.

23 **Folk R. L.**, **Ward W. C.**, Brazos River bar : a study in the significance of grain size parameters, *Journal of Sedimentary Petrology*, **1957**, vol. **27**, pp. 3-26.

24 **Klingbeil R.**, *Outcrop analogue studies - Implications for groundwater flow and contaminant transport in heterogeneous glaciofluvial quaternary deposits*, Dissertation, Department of Applied Geology, University of Tübingen, Germany, **1998**, 111 pages.

25 **Lassabatère L.**, **Angulo-Jaramillo R.**, **Soria Ugalde J. M.**, **Cuenca R.**, **Braud I.**, **Haverkamp R.**, Beerkan estimation of soil transfer parameters through infiltration experiments - BEST, *Soil Science Society of America Journal*, **2006**, vol. **70**, pp. 521-532.

26 **Braud I.**, **De Condappa D.**, **Soria J. M.**, **Haverkamp R.**, **Angulo-Jaramillo R.**, **Galle S.**, **Vauclin M.**, Use of Scaled forms of the infiltration equation for the estimation of unsaturated soil hydraulics properties (the *Beerkan* method), *European Journal of Soil Science*, **2005**, vol. **56**, pp. 361-374.

27 **Haverkamp R.**, **Debionne S.**, **Viallet P.**, **Angulo-Jaramillo R.**, **De Condappa D.**, *Soil properties and moisture movement in the unsaturated zone.* In : J. W. Delleur (Ed), The Handbook of Groundwater Engineering, CRC Press, **2007**, Chapitre **6**, pp. 6.1-6.59.

28 **Haverkamp R.**, **Leij F. J.**, **Fuentes C.**, **Sciortino A.**, **Ross P. J.**, Soil Water Retention : I. Introduction of a Shape Index, *Soil Science Society of America Journal*, **2005**, vol. **69**, pp. 1881-1890.

29 **Leij F. J.**, **Haverkamp R.**, **Fuentes C.**, **Zataraín F.**, **Ross P. J.**, Soil Water Retention : II. Derivation and Application of Shape Index, *Soil Science Society of America Journal*, **2005**, vol. **69**, pp. 1891-1901.

30 **Haverkamp R.**, **Ross P. J.**, **Smetten K. R. J.**, **Parlange J.-Y.**, Three-dimensional analysis of infiltration from the disc infiltromter. 2. Physically based infiltration equation, *Water Resources Research*, **1994**, vol. **30**, pp. 2931-2935.

31 **Arya L. M.**, **Paris J. F.**, A physicoempirical model to predict the Soil Moisture Characteristic from particle-size distribution and bulk-density data, *Soil Science Society of America Journal*, **1981**, vol. **45**, pp. 1023-1030.

32 **Jakobsen P. R.**, **Overgaard T.**, Georadar facies and glaciotectonic structures in ice marginal deposits, northwest Zealand, Denmark, *Quaternary Science Reviews*, **2002**, vol. **21**, nº **8-9**, pp. 917-927.

33 **Kostic B.**, **Becht A.**, **Aigner T.**, 3-D sedimentary architecture of a Quaternary gravel delta (SW-Germany) : Implications for hydrostratigraphy, *Sedimentary Geology*, **2005**, vol. **181**, nº **3-4**, pp. 147-171.

34 **Goutaland D.**, **Winiarski T.**, **Bièvre G.**, **Buoncristiani J.-F.**, Intérêt de l'approche sédimentologique en matière d'infiltration d'eaux pluviales. Caractérisation par radar géologique, *Techniques Sciences Méthodes*, **2005**, vol. **10**, pp. 71-79.

35 **Simunek J.**, **Sejna M.**, **van Genuchten M. T.**, The HYDRUS-2D software package for simulating two-dimensional movement of water, heat, and multiple solutes in variably saturated media, *Version 2.0, IGWMC-TPS-53, International Groundwater Modeling Center, Colorado School of Mines, Golden, Colorado*, **1999**, 251 pages.

36 **Hollenbeck K. J.**, **Simunek J.**, **van Genuchten M. T.**, RETCML : Incorporating maximum-likelihood estimation principles in the RETC soil hydraulic parameter estimation code, *Computers & Geosciences*, **2000**, vol. **26**, nº **3**, pp. 319-327.

37 **Siegenthaler C.**, **Huggenberger P.**, *Pleistocene Rhine gravel : deposits of a braided river system with dominant pool preservation*. In : J. L. Best and C. S. Bristow (Ed), Braided rivers, Geological Society Special Publication, **1993**, vol. **75**, pp. 147-162.

38 **Jussel P.**, **Stauffer F.**, **Dracos T.**, Transport modeling in heterogeneous aquifers : 1. Statistical description and numerical generation of gravel deposits, *Water Resources Research*, **1994**, vol. **30**, nº **6**, pp. 1803-1817.

39 **Chapuis R. P.**, **Aubertin M.**, On the use of the Kozeny-Carman equation to predict the hydraulic conductivity of soils, *Canadian Geotechnical Journal*, **2003**, vol. **40**, pp. 616-628.

40 **Anderson M. P.**, **Aiken J. S.**, **Webb E. K.**, **Mickelson D. M.**, Sedimentology and hydrogeology of two braided stream deposits, *Sedimentary Geology*, **1999**, vol. **129**, n° **3-4**, pp. 187-199.

41 **Bersezio R.**, **Bini A.**, **Giudici M.**, Effects of sedimentary heterogeneity on groundwater flow in a Quaternary pro-glacial delta environment : joining facies analysis and numerical modelling, *Sedimentary Geology*, **1999**, vol. **129**, n° **3-4**, pp. 327-344.

42 **Ganaye A.**, **Winiarski T.**, **Goutaland D.**, Impact d'un bassin d'infiltration d'eaux pluviales sur sa zone non saturée : relation entre la rétention des métaux et l'hétérogénéité de la formation fluvioglaciaire, *Novatech'2007*, Lyon, France, **2007**, vol. **2**, pp. 835-842.

43 **Kowalsky M. B.**, **Rubin Y.**, **Dietrich P.**, *The use of ground penetrating radar for characterizing sediments under transient flow conditions*. In : J. S. Bridge and D. W. Hyndman (Ed), Aquifer Characterization, **2004**, **80**, pp. 107-127.